Supporting Information

GSH-activated MRI-guided enhanced photodynamic- and chemo-combination therapy with a MnO_2-coated porphyrin metal organic framework

Xue-Tao Tian,[a] Pei-Pei Cao,[b] Hui Zhang,[a] Yu-Hao Li [b] and Xue-Bo Yin*[a]

[a] State Key Laboratory of Medicinal Chemical, Biology and Tianjin Key Laboratory of Biosensing and Molecular Recognition, College of Chemistry, Nankai University, Tianjin, 300071, China. E-mail: xbyin@nankai.edu.cn

[b] Tianjin Key Laboratory of Tumor Microenvironment and Neurovascular Regulation, School of Medicine, Nankai University, Tianjin, 300071, China.

*E-mail: xbyin@nankai.edu.cn

Table of contents

respectively.

Fig. S8 (a) Quantification of MR signals at muscle and tumor of the mice pre-and 30 min post-injection based on images in Fig. 2c. (b) Quantification of T1 MR signals from tumor areas in the mice at different time points based on images in Fig. 2d. (c) Coronal MR images of 4T1 tumor-bearing mice before and after intravenous administration of PCN@MnO_2@PAH. The regions with circles are kidneys and white arrows indicate livers. (d) Quantification of MR signals at kidney and liver of the mice pre-and post-injection based on images in (c).

Fig. S9 Biodistribution of PCN@MnO_2@PAH in mice at 24 h after intravenously injection. The concentration of Mn was measured by ICP.

Fig. S10 Absorbance spectra of ABDA incubated with PCN-222 in the presence of 10 mM GSH under the irradiation of 655 nm light at different time.

Fig. S11. DOX release profiles of DOX@PCN@MnO_2@PAH in physiological environment (pH 7.0, 10 mM HEPES buffer) and tumor microenvironment (pH 4.0, 10 mM HAc-NaAc buffer, 10 mM GSH).

Fig. S12 Cytotoxicity of PCN@MnO_2@PAH at different concentrations for HeLa cells for 6 h.

Fig. S13 Confocal fluorescence images of (a) 4T1 cells and (b) HeLa cells incubated with PCN@MnO_2@PAH for 2, 4 and 6 h. Blue and red signals represent DAPI and PCN@MnO_2@PAH fluorescence, respectively. The excitation wavelengths for DAPI and

PCN@MnO_2@PAH were set at 405 nm and 559 nm, respectively. Scale bars: 50 μm.

Fig. S14 Confocal fluorescence images of 4T1 cells incubated with PCN@MnO_2@PAH at various concentrations (0, 50, 100, 200, 400 μg mL^{-1}). Blue and red signals represent DAPI and PCN@MnO_2@PAH fluorescence, respectively. The excitation wavelengths for DAPI and PCN@MnO_2@PAH were set at 405 nm and 559 nm, respectively. Scale bars: 50 μm.

Fig. S15 Confocal fluorescence images of HeLa cells incubated with PCN@MnO_2@PAH at various concentrations (0, 50, 100, 200, 400 μg mL^{-1}). Blue and red signals represent DAPI and PCN@MnO_2@PAH fluorescence, respectively. The excitation wavelengths for DAPI and PCN@MnO_2@PAH were set at 405 nm and 559 nm, respectively. Scale bars: 50 μm.

Fig. S16 Viability of 4T1 cells after different treatments from MTT assay to reveal their cytotoxicity. (1) PCN-222 with 655 nm laser irradiation, (2) PCN@MnO_2@PAH with 655 nm laser irradiation, (3) DOX@PCN@MnO_2@PAH without laser irradiation, and (4) DOX@PCN@MnO_2@PAH with 655 nm laser irradiation, (400 μg mL^{-1}, based on PCN-222).

Fig. S17 Time dependent relative body weight curves of mice in each experiment group. W_0 and W represent body weights before and after treatment with corresponding nanoparticles.

Fig. S18 H&E-stained images of main organs harvested from mice at 15 days post-treatment.

Fig. S19 The IC50 values of PCN-222 (a) and PCN@MnO_2@PAH (b) under 655 nm light irradiation from MTT assay based on Fig. 3d.

Fig. S20 Viability of 4T1 cells after treated with TCPP under 655 nm light irradiation from MTT assay to reveal their cytotoxicity. The above concentration of TCPP is based on the concentration of PCN-222. PCN-222 contains 66% of TCPP.

MATERIALS AND METHODS

Materials. $ZrCl_4$ was obtained from Alfa-Asia, Tianjin, China. 5,10,15,20–Tetrakis(4-carboxyl)-21H,23H-porphine (TCPP) was obtained from TCI Chemical Ind. Develop Co., Shanghai. China. Benzoic acid (BA, 98.5 %) was purchased from Guangfu Fine Chemical Research Institute, Tianjin, China. Poly(allylamine hydrochloride) (PAH, MW= 15,000-20000) was purchased from Keychems, Tianjin, China. Glutathione (GSH) was purchased from J&K chemical CO.. Potassium permanganate ($KMnO_4$) was obtained from Bohua Chemical Reagents Co., Tianjin, China. Dimethylformamide (DMF) and other solvents were from Concord Reagent Co., Tianjin, China. 9,10-anthracenediyl-bis (methylene)dimalonic acid (ABDA) was purchased from Aladdin biotechnology Co., Shanghai, China. 3,6-Di(O-acetyl)-4,5-bis[N,N-bis(carboxymethyl)aminomethyl] fluorescein (Calcein-AM) and Propidium iodide (PI) were obtained from Yeasen, Shanghai, China. All reactants were analytic grade and were used as purchased without further purification. Ultra-pure water was prepared with an Aquapro system (18.25 MΩ).

Instrumentation and characterization. UV-Vis absorption spectra were measured with a UV-2450-visible spectrophotometer (Shimadzu, Japan). The fluorescence spectra were performed on a FL-4600 Fluorescence Spectrometer (Hitachi, Japan) with a quartz cell. The FT-IR spectra were obtained by Bruker TENSOR 27 FT-IR spectrometer. Thermogravimetric analysis (TGA) was performed on a PTC-10ATG-DTA analyzer heated from 20 °C at a ramp rate of 10 °C min^{-1} under air.

Transmission electron microscopy (TEM) images and energy-dispersive X-ray analysis (EDX) were obtained on Tecnai G2 F20, FEI Co., America operated at 200 kV. The powder

XRD patterns were recorded on a D/max-2500 diffractometer (Rigaku, Japan) with Cu Kα radiation (λ=1.5418 Å). The content of Zr and Mn were measured by Inductively Coupled Plasma Atomic Emission Spectroscopy (ICP-AES), IRIS advantage, Thermo, USA. Hydrodynamic size distribution (DLS) and zeta potential were measured by a Zetasizer Nano ZS90, Malvern, UK. The MR images and transverse relaxivity time were performed by a MRI system (1.2 T, Huantong, Shanghai, China). X-ray photoelectron spectra (XPS) were performed on an Axis Ultra DLD with a monochromatized Al Kα radiation source.

Methods. 72 nm PCN-222 (the average sizes along the major axis). Nano-PCN-222 was synthesized by the previous literature with slight modifications. The mixtures of zirconium tetrachloride ($ZrCl_4$) (30 mg) and 5,10,15,20–tetrakis(4-carboxyl)-21H, 23H-porphine (H_2TCPP) (10 mg) were dissolved in N,N-dimethylformamide (DMF) (12 mL) by sonication for 16 min. And then benzoic acid (BA) (400 mg) was ultrasonically dissolved in the above solution for 8 min. The mixtures were heated in the 120 °C oven for 24 h. After the reaction cooled to room temperature, the resulting precipitate was washed three times with DMF, ethanol and water. The resulting nano PCN-222 was suspended in water for further application and characterization.

1.8 μm PCN-222 (the average sizes along the major axis): The mixtures of $ZrCl_4$ (30 mg) and H_2TCPP (10 mg) were dissolved in DMF (6 mL) by sonication for 16 min. And then BA (400 mg) was ultrasonically dissolved in the above solution for 8 min. The mixtures were heated in the 120 °C oven for 24 h. After the reaction cooled to room temperature, the resulting precipitate was washed three times with DMF, ethanol and water.

250 nm PCN-222 (the average sizes along the major axis): The mixtures of $ZrCl_4$ (30 mg) and H_2TCPP (10 mg) were dissolved in DMF (8 mL) by sonication for 16 min. And then BA (400 mg) was ultrasonically dissolved in the above solution for 8 min. The mixtures were heated in the 120 °C oven for 24 h. After the reaction cooled to room temperature, the resulting precipitate was washed three times with DMF, ethanol and water.

139 nm PCN-222 (the average sizes along the major axis): The mixtures of $ZrCl_4$ (30 mg) and H_2TCPP (10 mg) were dissolved in DMF (10 mL) by sonication for 16 min. And then BA (400 mg) was ultrasonically dissolved in the above solution for 8 min. The mixtures were heated in the 120 °C oven for 24 h. After the reaction cooled to room temperature, the resulting precipitate was washed three times with DMF, ethanol and water.

30 nm PCN-222 (the average sizes along the major axis): The mixtures of $ZrCl_4$ (30 mg) and H_2TCPP (10 mg) were dissolved in DMF (28 mL) by sonication for 16 min. And then BA (400 mg) was ultrasonically dissolved in the above solution for 8 min. The mixtures were heated in the 120 °C oven for 24 h. After the reaction cooled to room temperature, the resulting precipitate was washed three times with DMF, ethanol and water.

Synthesis of PCN@MnO_2@PAH. In a typical synthesis, 18.4 mg as-prepared PCN-222 nanoparticles (72 nm) were first dispersed into water (5 mL) and sonicated for 8 min. Aqueous PAH (MW= 15,000-20000, 5 mL, 18.4 mg) is adjusted to pH 7.23 with the NaOH solution (1 M). Then the PAH solution was added into the above PCN-222 solution and mixed at room temperature under stirring overnight. The obtained PCN@PAH was washed three times with water. Subsequently, as-prepared PCN@PAH nanoparticles was re-dispersed into water (24 mL) and sonicated for 8 min to ensure that the PCN@PAH nanoparticles were

suspended well in the solution. Aqueous $KMnO_4$ (1 mg mL^{-1}, 8 mL) was dropwise added into the above PCN@PAH solution under vigorously stirring. After stirring for 30 min, the obtained PCN@MnO_2 was centrifuged and washed with DI water for three times. As-prepared PCN@MnO_2 nanoparticles were dispersed into water (10 mL) and sonicated for 8 min. Then 20 mL of PAH solution (5 mg mL^{-1}, pH 7.23) was added into the above PCN@MnO_2 solution under sonication. After stirring overnight, the PCN@MnO_2@PAH nanoparticles were centrifuged and washed with DI water for three times.

DOX uptake experiment. 4 mg PCN@MnO_2@PAH nanoparticles were mixed 4 mL DOX•HCl solution (1 mg/mL) with agitating for 3 days. The amount of DOX in the supernatant solution was determined by UV-vis absorbance at 480 nm. The loading capacity (LC) was calculated with the followed formula: LC (wt%) =(weight of loaded DOX / the original mass of PCN@MnO_2@PAH) × 100%.

DOX-releasing experiment. To determine drug release, DOX@PCN@MnO_2@PAH was treated with normal physiological condition or tumor microenvironment solution. The released DOX was quantified by UV-vis absorbance at 480 nm.

In-vitro **singlet oxygen generation.** To determine GSH depletion-enhanced PDT ability, ABDA was used as the indicator to determine the generation of $^1O_2$ using UV-vis spectrophotometer. The PCN@MnO_2@PAH (24 μg, equal to 20 μg PCN-222) or PCN-222 (20 μg) was incubated with 10 mM GSH in phosphate buffer saline (PBS) buffers (pH = 7.4). After ABDA (200 μM) being added, the above solutions were irradiated with a 655 nm laser (light intensity 94 mW/cm^2). At each 5 min interval, the UV-vis absorption spectra of solutions at 378 nm were recorded.

***In vitro* GSH-activated MRI contrast performance.** *In vitro* MR imaging experiments were performed on a 1.2 T MR imaging system (Huantong, Shanghai, China). The T1- and T2-weighted MRI values of PCN@MnO_2@PAH at different concentrations in the absence or presence of 10 mM GSH were determined. The T1- and T2-weighted MR imaging of the above materials were acquired on 50 mm animal coil, using a fat-saturated 3D gradient echo imaging sequence (spin-echo T1-weighted MR sequence, TR/TE = 100.0/8.8 ms, FOV = 100 ×50 mm^2, matrix = 512 × 512, slice thickness = 1 mm, 30.0 °C; spin-echo T2-weighted MR sequence, TR/TE = 5000/64.6 ms, FOV = 50 × 80 mm^2, matrix = 512 × 256, slice thickness = 0.4 mm, 30.0 ^oC).

Cell culture. Murine breast cancer cell line (4T1) was obtained from the Chinese Academy of Sciences, Beijing, China. 4T1 cells were maintained in complete 1640 medium (1640, Biological Industries, Israel) supplemented with 10 % fetal bovine serum (FBS, BI, Israel) and 1 % penicillin-streptomycin solution (PS, Life technologies, America). The cell lines were maintained in HERAcell VIOS 150i CO_2 incubator (Thermo scientific, America) at 37 °C in a 5 % CO_2 atmosphere with 95 % humidity.

Human cervical cancer cell line (HeLa) was obtained from the Chinese Academy of Sciences, Beijing, China. Hela cells were maintained in complete DMEM medium (DMEM, Biological Industries, Israel) supplemented with 10 % fetal bovine serum (FBS, BI, Israel) and 1 % penicillin-streptomycin solution (PS, Life technologies, America). The cell lines were maintained in HERAcell VIOS 150i CO2 incubator (Thermo scientific, America) at 37 °C in a 5 % CO_2 atmosphere with 95 % humidity.

Intracellular Endocytosis of PCN@MnO_2@PAH. 4T1 cells were seeded in 24-well plates at a density of 4×10^4 cells per well, the plates were maintained at 37 °C in 5 % CO_2 air incubator for 24 h. HeLa cells were seeded in 24-well plates at a density of 4×10^4 cells per well, the plates were maintained at 37 °C in 5 % CO_2 air incubator for 24 h.

To examine the time-dependent uptake of cells by PCN@MnO_2@PAH nanoparticles, 4T1 cells and HeLa cells were incubated with PCN@MnO_2@PAH for 2, 4, and 6 h. Then the cells were fixed with 4 % paraformaldehyde in PBS for 20 min at room temperature. After washing with PBST (5 % Tween 20 in PBS) solution three times, the cell nuclei were stained with 4',6-diamidino-2-phenylindole (DAPI) and imaged by confocal laser scanning microscope (CLSM, Olympus FV1000).

To examine the concentration-dependent uptake of cells by PCN@MnO_2@PAH nanoparticles, 4T1 cells and HeLa cells were incubated with different concentrations of PCN@MnO_2@PAH (0, 50, 100, 200, and 400 μg mL^{-1}) for 6 h. Then the cells were fixed with 4 % paraformaldehyde in PBS for 20 min at room temperature. After washing with PBST solution three times, the cell nuclei were stained with DAPI and imaged by CLSM (Olympus FV1000).

Cytotoxicity assays. 4T1 cells (10^5 cells mL^{-1}) were incubated in 96-well microtiter plates for 3-(4,5-dimethylthiazol-2-yl)-2,5-diphenyltetrazolium bromide (MTT) assay. 4T1 cells were maintained at 37 °C in 5 % CO_2 incubator for 24 h. Then 4T1 cells were incubated with different concentration of PCN-222 or PCN@MnO_2@PAH (0, 50, 100, 200 and 400 μg mL^{-1}, based on PCN-222) for 12 h. After washing three times with PBS solution, PCN-222 and PCN@MnO_2@PAH groups were irradiated by a 655 nm laser (300 mW cm^{-2}) for 30 s.

Afterwards, 4T1 cells were maintained at 37 °C in 5 % CO_2 air incubator for another 12 h. 20 μL of MTT solution (5.0 mg mL^{-1}, BBS) was added to each well. After 3 h, the MTT solution was discarded, and the formazan crystals were dissolved into 150 μL dimethyl sulfoxide (DMSO). The cells viabilities were measured by the MTT assay.

For *in vitro* synergistic therapy, 4T1 cells were incubated with PCN-222 (with laser irradiation, 400 μg mL^{-1}), PCN@MnO_2@PAH (with laser irradiation, 400 μg mL^{-1}, based on PCN-222), and DOX@PCN@MnO_2@PAH (with or without laser irradiation, 400 μg mL^{-1}, based on PCN-222). The groups were treated with or without a 655 nm laser irradiation (300 mW cm^{-2}, 30 s). The cells were incubated for 12 h. The cell viabilities were measured by standard MTT assay.

Measurement of intracellular $^1O_2$ generation. 4T1 cells were incubated with PCN-222 or PCN@MnO_2@PAH (400 μg mL^{-1}, based on PCN-222) for 12 h. After washed three times with PBS solution, 500 μL 2',7'-dichlorofluorescein diacetate (DCFH-DA, 10 μM) was added into each well to incubate for 30 minutes. Then, the remaining DCFH-DA was discarded, and 4T1 cells were maintained in complete 1640 medium. PCN-222 and PCN@MnO_2@PAH groups were irradiated by a 655 nm laser (300 mW cm^{-2}) for 5 min, respectively. After photodynamic therapy, 4T1 cells were incubated for 15 min. CLSM images of cells were obtained at an excitation of 488 nm.

Dead /live cell double staining. 4T1 cells were incubated with PCN-222 or PCN@MnO_2@PAH (400 μg mL^{-1}, based on PCN-222) for 12h. After washed three times with PBS solution, PCN-222 and PCN@MnO_2@PAH groups were irradiated by a 655 nm laser (300 mW cm^{-2}) for 5 min, respectively. Then, the cells were all stained by the mixtures

of Calcein-AM (2 μM) and PI (4.5 μM) at 37 ºC for 30 min in the 1640 medium without FBS. After washed with PBS solution, the fluorescence images of the cells were immediately obtained by CLSM. Calcein-AM and PI were excited at 480 nm and 543 nm, and the corresponding emissions were recorded between 500-550 nm and 580-650 nm, respectively.

Animal experiments

Female Balb/c mice (18-22 g) were purchased from the Institute of Hematology & Hospital of Blood Disease, Chinese Academy of Medical Sciences & Peking Union Medical College, China. All mice experimental protocols were approved by the Institutional Animal Care Committee of Nankai University.

***In vivo* GSH-activated MRI contrast performance.** MR imaging was performed on a 3.0 T MR imaging system (GE Signa Excite). 100 μL PCN@MnO_2@PAH (2μg μL^{-1}) solutions were in situ injected into the tumor (right side) and the muscle (left side) of 4T1 tumor-bearing mice, respectively. Then the MRI images of mice at selected time points were recorded to observe the GSH-activated MRI contrast performance in tumor site.

For *in vivo* MR imaging, 100 μL PCN@MnO_2@PAH (2 μg μL^{-1}) solutions were injected into a 4T1 tumor-bearing mice intravenously. At different time points (0, 15 min, 30 min, 2.5 h, and 24 h) post-injection, the T1-weighted MR images were recorded.

***In vivo* cancer treatment.** 4T1 tumor-bearing mice (18-22 g) as model were randomly divided into 5 groups, including (1) saline as control, (2) PCN-222 (200 μg) with laser irradiation for PDT, (3) PCN@MnO_2@PAH (200 μg, based on PCN-222) with laser irradiation for enhanced PDT, (4) DOX@PCN@MnO_2@PAH (200 μg, based on PCN-222)

without laser irradiation for chemotherapy, and (5) DOX@PCN@MnO_2@PAH (200 μg, based on PCN-222) with laser irradiation for PDT-chemotherapy synergetic therapy. Five groups of mice were intravenous injected with corresponding nanomaterials at first day and third day. At 1 h post-injection, the tumors of mice in group 2, 3 and 5 were irradiated by 655 nm laser (300 mW cm^{-2}) for 15 min. The tumor sizes and body weights of mice were monitored every two days. The tumor and main organ slices of mice were stained by Hematoxylin and eosin (H&E). The H&E stained images were used to investigate the therapeutic efficacy of different groups**.**

Equilibrium of PCN-222 formation

The formation mechanism of PCN-222 was investigated in combination with Zhou's results.[1] To obtain PCN-222, $Zr_6(BA)_{12}$ was first obtained through the coordination of benzoic acid (BA) and Zr_6 clusters. Then, benzoic acid was replaced from the as-formed complexes by TCPP with competitive coordination effect.[2-4] Finally, $Zr_6(TCPP)_2$ was obtained as PCN-222 monomer, as summarized in eqn (S1). The change of any parameter that affects the balance among the precursors may generate impure phase of the products. Thus, the strategy of decrease the concentration of the whole system with their fixed ratio was selected. Interestingly, if the system is diluted to 1/n, the number of PCN-222 nucleus increases sharply as illustrated in eqn (S2), giving the smaller particles without impurity phase. Therefore, the formation of PCN-222 is governed by nucleation-growth mechanism and diluted solution yields much more crystal nuclei with slow growth to form the product with small size.

$$Zr_6(BA)_{12}+2TCPP \xrightarrow{K} Zr_6(TCPP)_2+12BA$$

$$[PCN\text{-}222_{monomer}]=[Zr_6(TCPP)_2]=\frac{K\times[Zr_6(BA)_{12}]\times[TCPP]^2}{[BA]^{12}} \quad \text{(eqn S1)}$$

$$PCN\text{-}222_{monomer}=[Zr_6(TCPP)_2]$$

$$=\frac{K\times[Zr_6(BA)_{12}\times\frac{1}{n}]\times[TCPP\times\frac{1}{n}]^2}{[BA\times\frac{1}{n}]^{12}}$$

$$=\frac{K\times[Zr_6(BA)_{12}]\times[TCPP]^2}{[BA]^{12}}\times n^9 \quad \text{(eqn S2)}$$

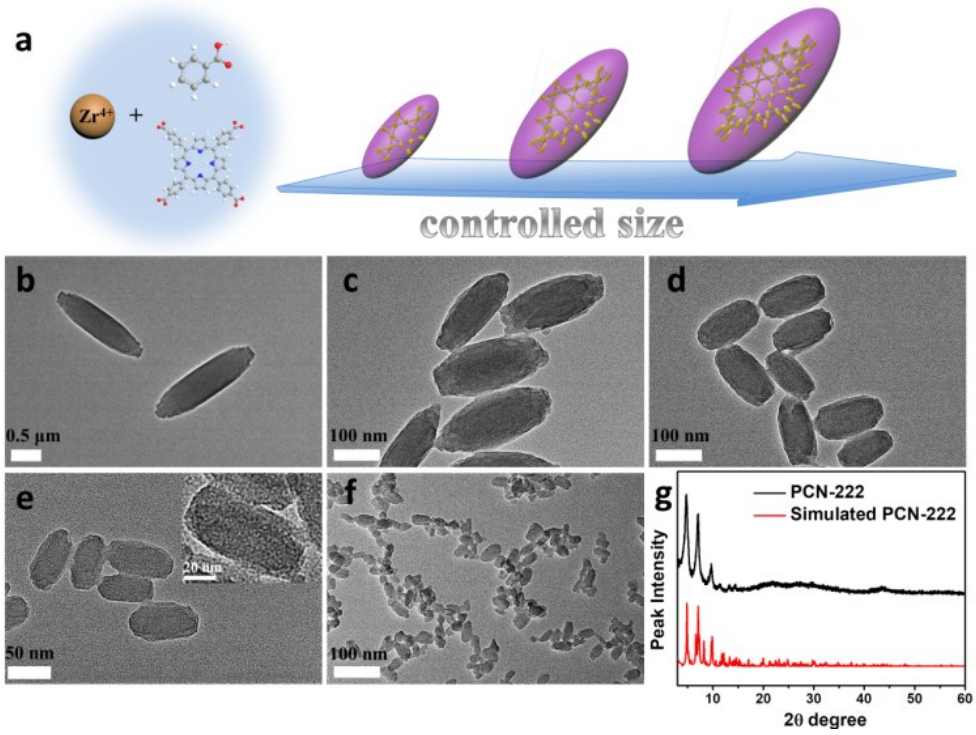

Fig. S1 (a) Schematic representation for the preparation of PCN-222 with different sizes. TEM images revealed that PCN-222 with the size of (b) 1.8 μm, (c) 250 nm, (d) 139 nm, (e) 72 nm, (f) 30 nm was synthesized with 30 mg $ZrCl_4$, 10 mg TCPP, and 400 mg benzoic acid in 6, 8, 10, 12, and 28 mL DMF at 120 °C, respectively. (g) PXRD of 72 nm PCN-222 and simulated data from single crystalline PCN-222.

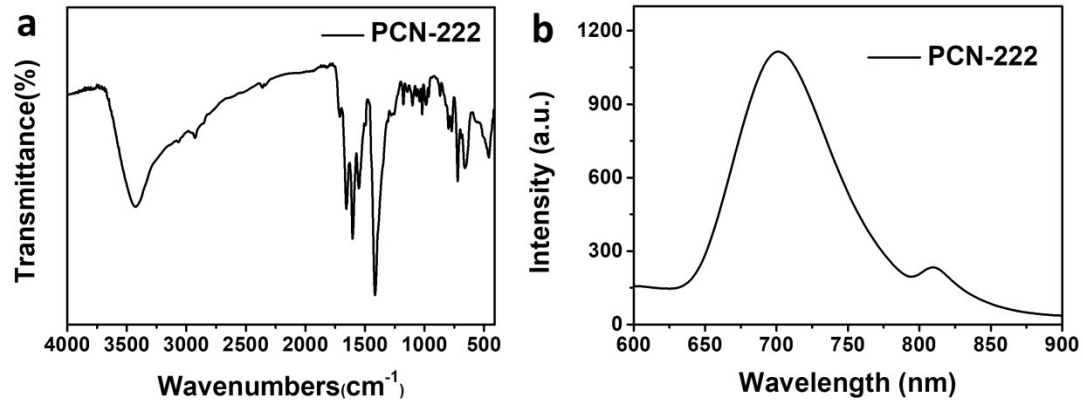

Fig. S2 (a) FT-IR spectrum of 72 nm PCN-222. (b) Fluorescence spectrum of 72 nm PCN-222 (λ_{ex} = 530 nm).

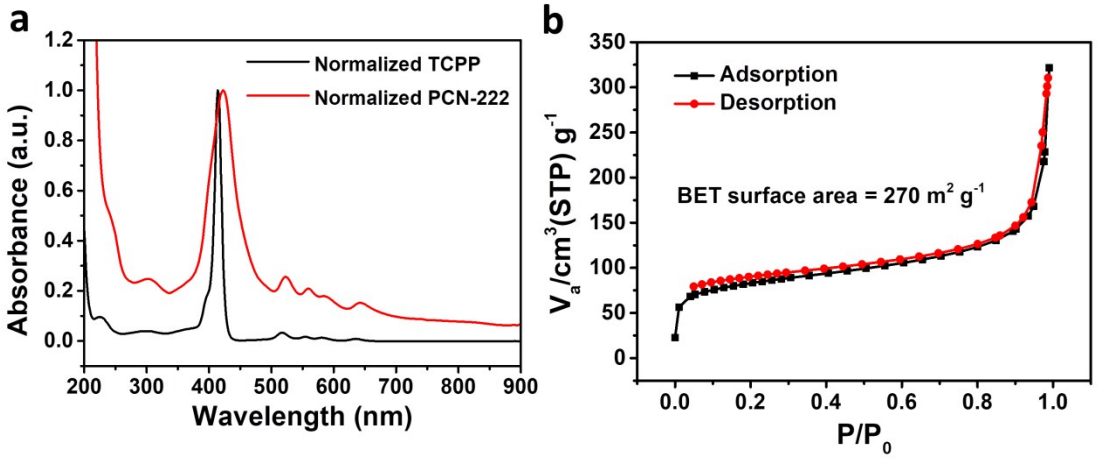

Fig. S3 (a) UV-vis spectra of TCPP and PCN-222. (b) Nitrogen adsorption/desorption isotherms performed at 77 K of the 72 nm PCN-222 samples.

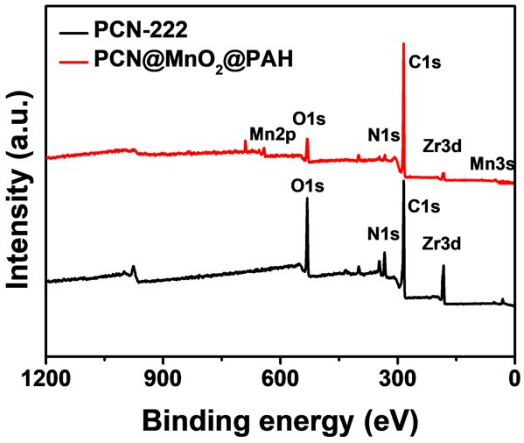

Fig. S4 XPS wide spectra of 72 nm PCN-222 and PCN@MnO_2@PAH.

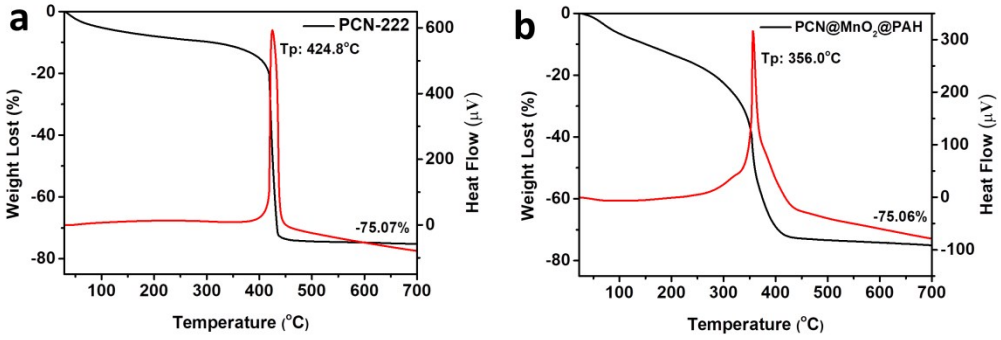

Fig. S5 The thermogravimetric analysis of 72 nm PCN-222 (a) and PCN@MnO_2@PAH (b).

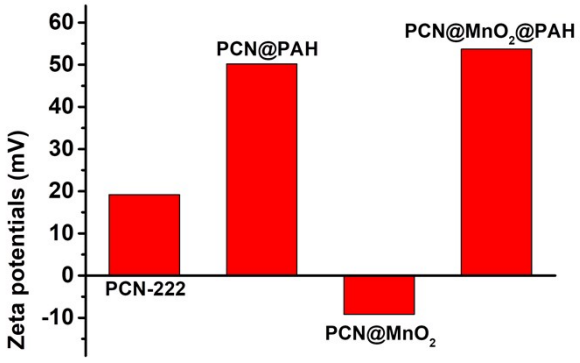

Fig. S6 Zeta potentials for nanoparticles measured at each synthesis step.

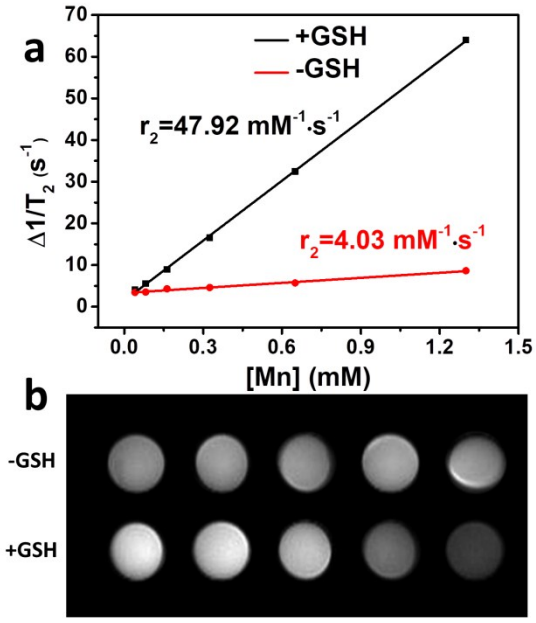

Fig. S7 (a) T2 relaxation rates versus Mn concentration for PCN@MnO_2@PAH solution (red lines) and PCN@MnO_2@PAH solution treated with GSH (black lines). (b) T2-weighted MR images of PCN@MnO_2@PAH solution with various concentrations obtained from (a). The concentrations of Mn^{2+} are 0.0406, 0.0812, 0.162, 0.325, and 0.650 mM from left to right, respectively.

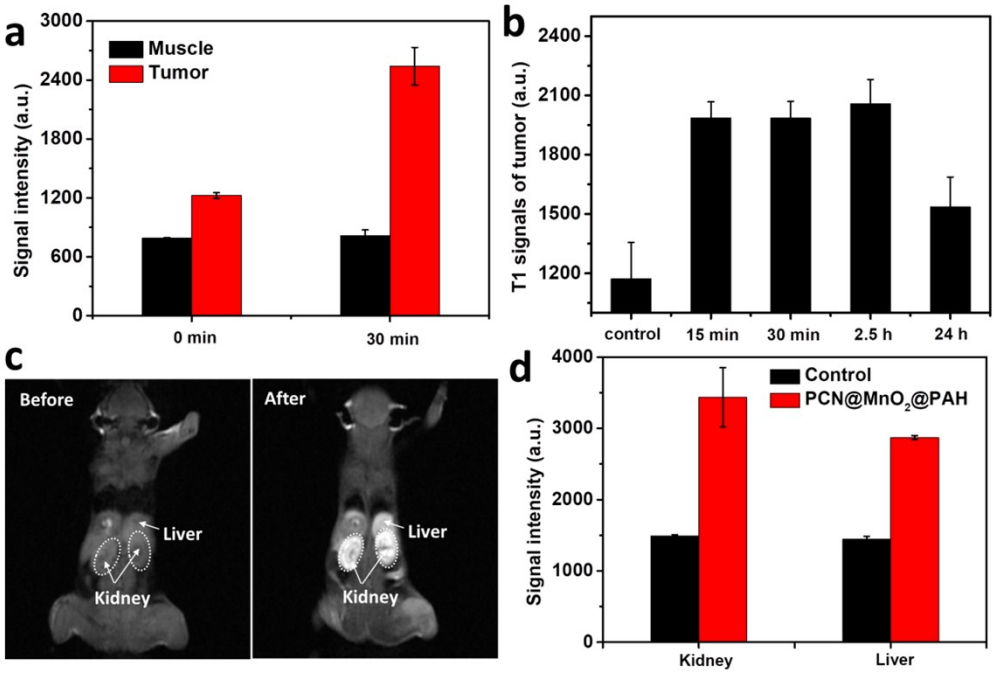

Fig. S8 (a) Quantification of MR signals at muscle and tumor of the mice pre-and 30 min post-injection based on images in Fig. 2c. (b) Quantification of T1 MR signals from tumor areas in the mice at different time points based on images in Fig. 2d. (c) Coronal MR images of 4T1 tumor-bearing mice before and after intravenous administration of PCN@MnO_2@PAH. The regions with circles are kidneys and white arrows indicate livers. (d) Quantification of MR signals at kidney and liver of the mice pre-and post-injection based on images in (c).

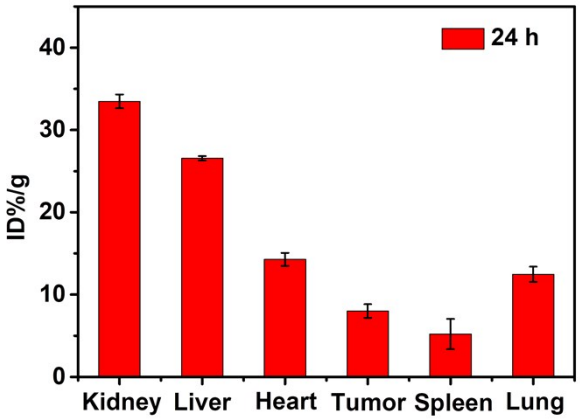

Fig. S9 Biodistribution of PCN@MnO_2@PAH in mice at 24 h after intravenously injection. The concentration of Mn was measured by ICP.

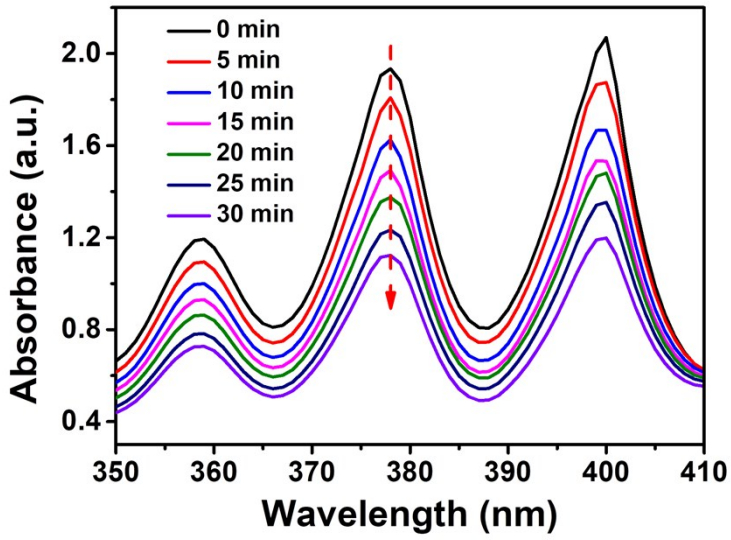

Fig. S10 Absorbance spectra of ABDA incubated with PCN-222 in the presence of 10 mM GSH under the irradiation of 655 nm light at different time.

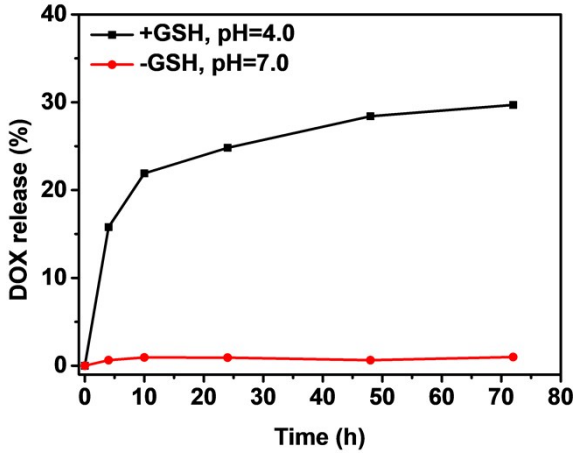

Fig. S11. DOX release profiles of DOX@PCN@MnO_2@PAH in physiological environment (pH 7.0, 10 mM HEPES buffer) and tumor microenvironment (pH 4.0, 10 mM HAc-NaAc buffer, 10 mM GSH).

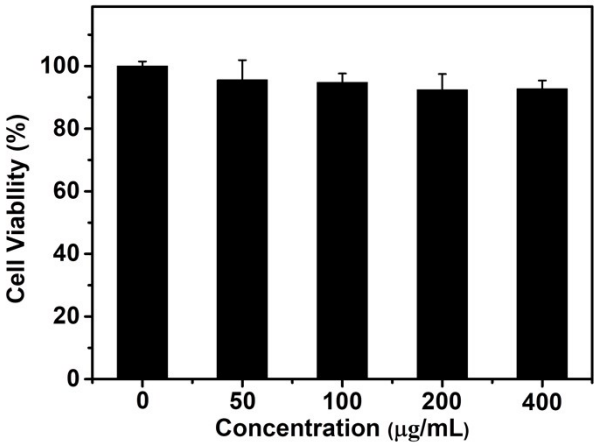

Fig. S12 Cytotoxicity of PCN@MnO_2@PAH at different concentrations for HeLa cells for 6 h.

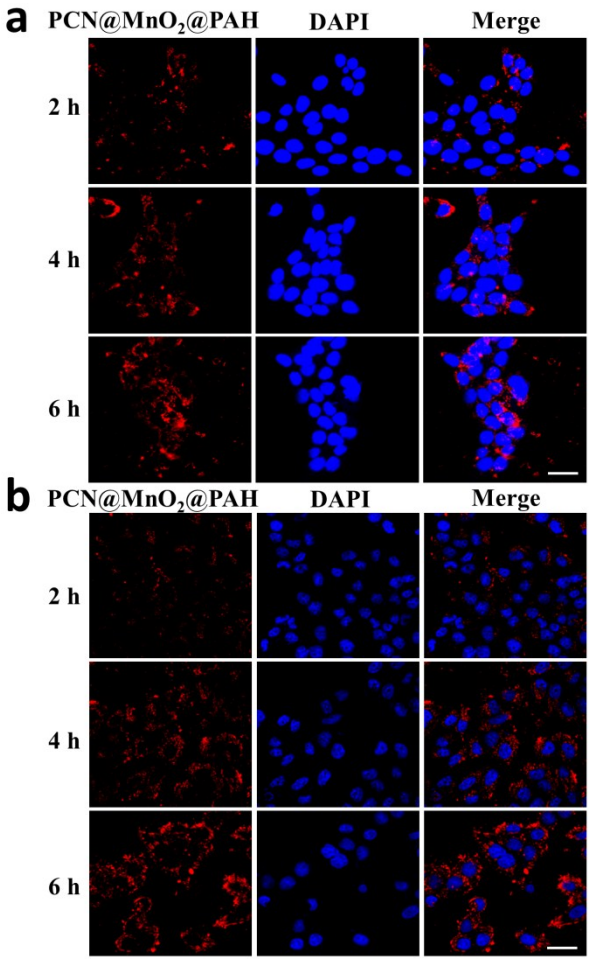

Fig. S13 Confocal fluorescence images of (a) 4T1 cells and (b) HeLa cells incubated with PCN@MnO_2@PAH for 2, 4 and 6 h. Blue and red signals represent DAPI and PCN@MnO_2@PAH fluorescence, respectively. The excitation wavelengths for DAPI and PCN@MnO_2@PAH were set at 405 nm and 559 nm, respectively. Scale bars: 50 μm.

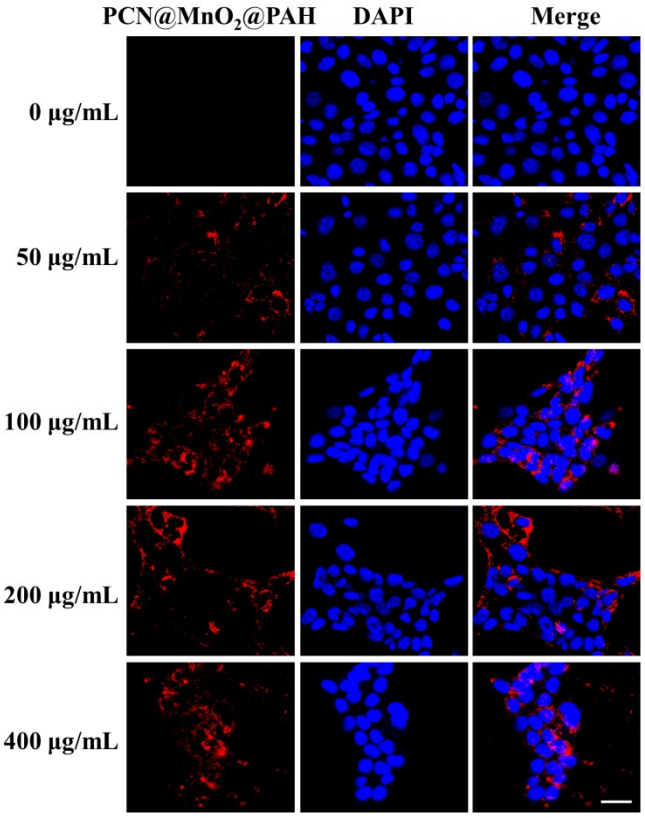

Fig. S14 Confocal fluorescence images of 4T1 cells incubated with PCN@MnO_2@PAH at various concentrations (0, 50, 100, 200, 400 μg mL^{-1}). Blue and red signals represent DAPI and PCN@MnO_2@PAH fluorescence, respectively. The excitation wavelengths for DAPI and PCN@MnO_2@PAH were set at 405 nm and 559 nm, respectively. Scale bars: 50 μm.

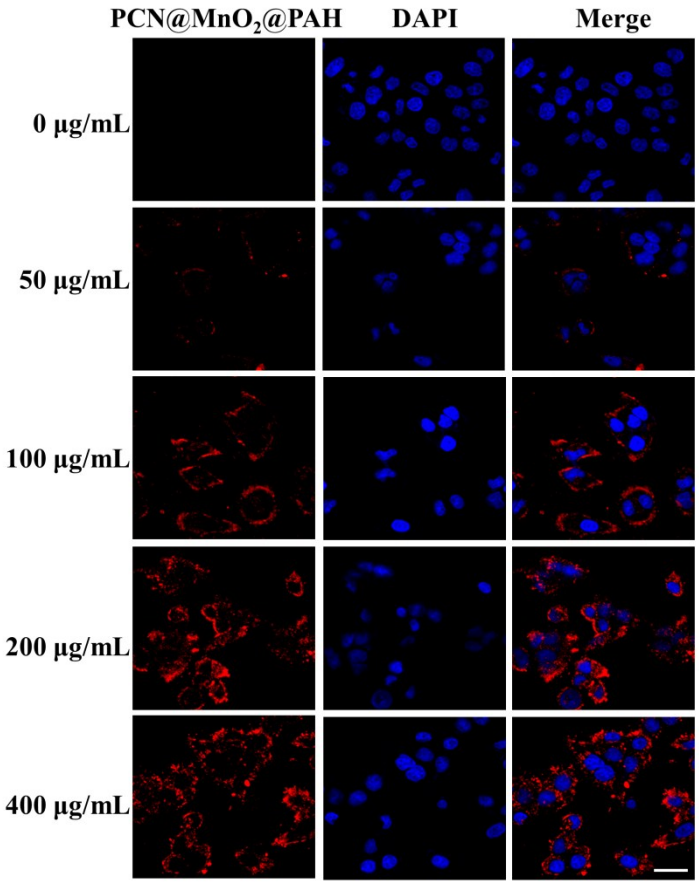

Fig. S15 Confocal fluorescence images of HeLa cells incubated with PCN@MnO_2@PAH at various concentrations (0, 50, 100, 200, 400 μg mL^{-1}). Blue and red signals represent DAPI and PCN@MnO_2@PAH fluorescence, respectively. The excitation wavelengths for DAPI and PCN@MnO_2@PAH were set at 405 nm and 559 nm, respectively. Scale bars: 50 μm.

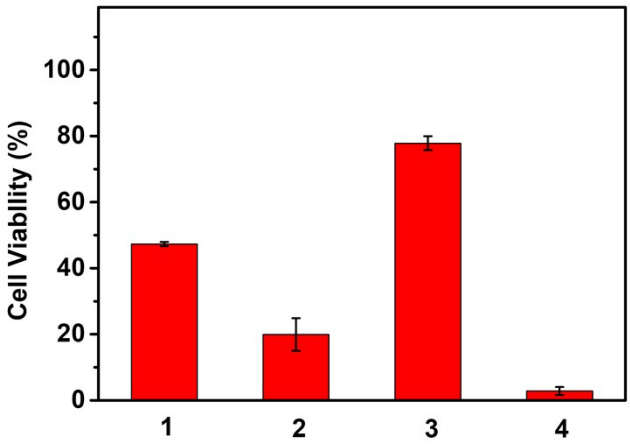

Fig. S16 Viability of 4T1 cells after different treatments from MTT assay to reveal their cytotoxicity. (1) PCN-222 with 655 nm laser irradiation, (2) PCN@MnO_2@PAH with 655 nm laser irradiation, (3) DOX@PCN@MnO_2@PAH without laser irradiation, and (4) DOX@PCN@MnO_2@PAH with 655 nm laser irradiation, (400 μg mL^{-1}, based on PCN-222).

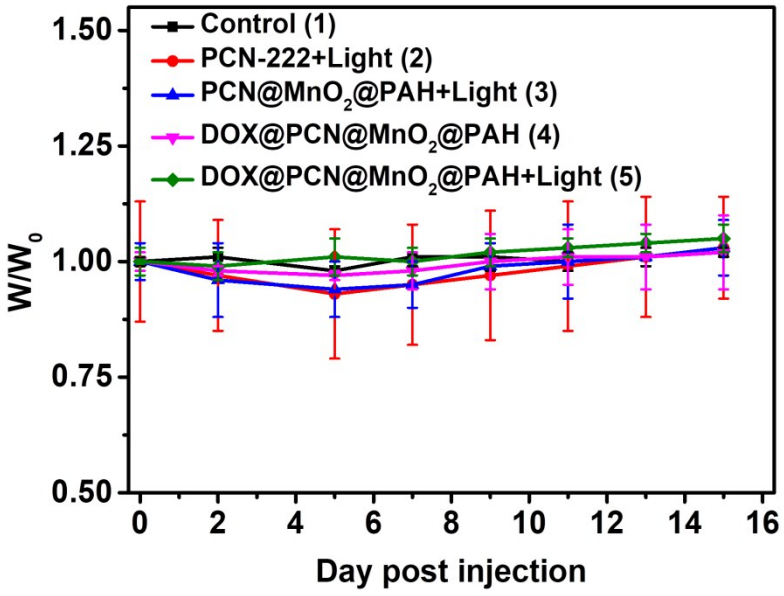

Fig. S17 Time dependent relative body weight curves of mice in each experiment group. W_0 and W represent body weights before and after treatment with corresponding nanoparticles.

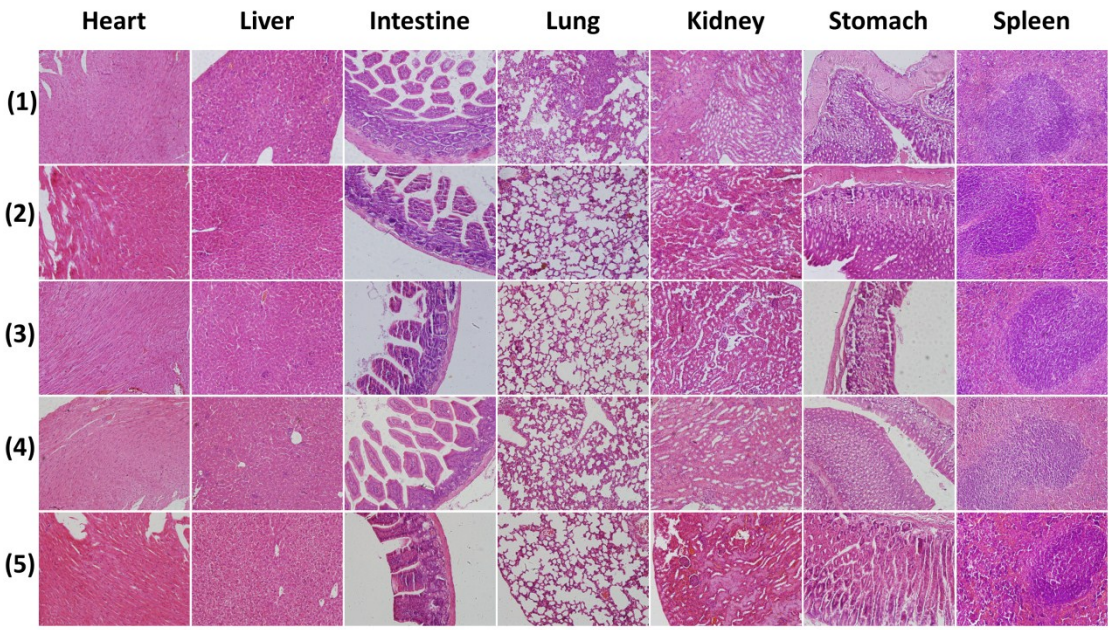

Fig. S18 H&E-stained images of main organs harvested from mice at 15 days post-treatment.

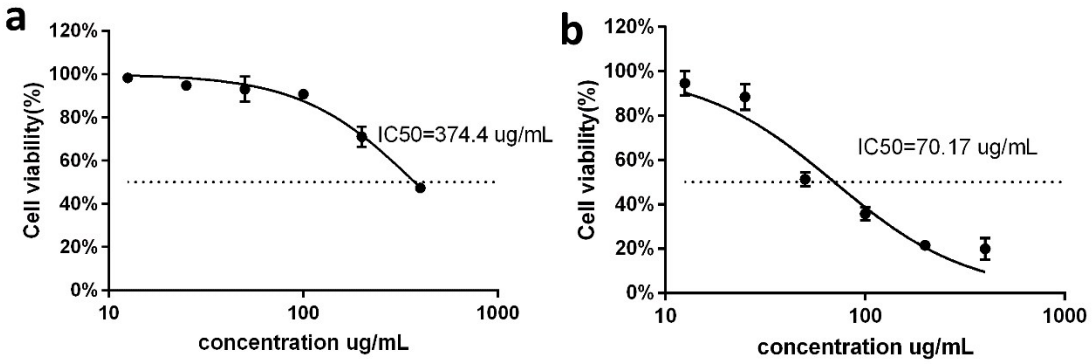

Fig. S19 The IC50 values of PCN-222 (a) and PCN@MnO_2@PAH (b) under 655 nm light irradiation from MTT assay based on Fig. 3d.

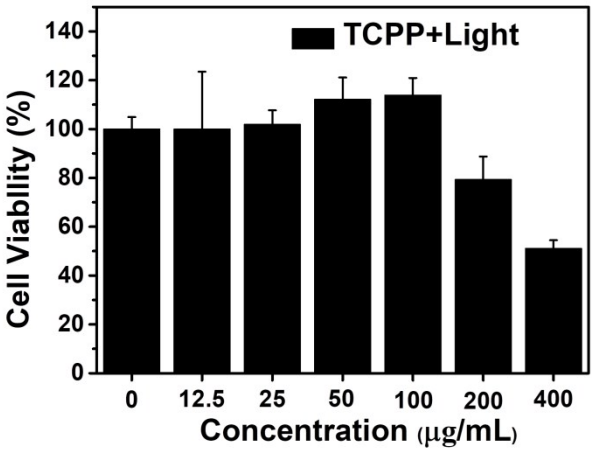

Fig. S20 Viability of 4T1 cells after treated with TCPP under 655 nm light irradiation from MTT assay to reveal their cytotoxicity. The above concentration of TCPP is based on the concentration of PCN-222. PCN-222 contains 66% of TCPP.

1. J. Park, Q. Jiang, D. Feng, L. Mao and H.-C. Zhou, *J. Am. Chem. Soc.*, 2016, **138**, 3518–3525.
2. D. Feng, K. Wang, Z. Wei, Y.-P. Chen, C. M. Simon, R. K. Arvapally, R. L. Martin, M. Bosch, T.-F. Liu, S. Fordham, D. Yuan, M. A. Omary, M. Haranczyk, B. Smit and H.-C. Zhou, *Nat. Commun.*, 2014, **5**, 5723.
3. A. Schaate, P. Roy, A. Godt, J. Lippke, F. Waltz, M. Wiebcke and P. Behrens, *Chem. Eur. J.*, 2011, **17**, 6643-6651.
4. T. Tsuruoka, S. Furukawa, Y. Takashima, K. Yoshida, S. Isoda and S. Kitagawa, *Angew. Chem. Int. Ed.*, 2009, **48**, 4739-4743.
5. W. Liu, Y.-M. Wang, Y.-H. Li, S.-J. Cai, X.-B. Yin, X.-W. He and Y.-K. Zhang, *Small*, 2017, **13**, 1603459.
6. M.-H. Pham, G.-T. Vuong, A.-T. Vu and T.-O. Do, *Langmuir*, 2011, **27**, 15261-15267.